Int. J. Electrochem. Sci., 15 **(2020)** 12475 – 12490, doi: 10.20964/2020.12.74

International Journal of
ELECTROCHEMICAL
SCIENCE
www.electrochemsci.org

Investigation of the Electrochemical Performance of Anode-Supported SOFCs under Steady-State Conditions

Yutao Lian, Minggang Zheng[*]

School of Mechanical and Electronic Engineering, Shandong Jianzhu University, Jinan, People's Republic of China
[*]E-mail: why1318@sdjzu.edu.cn

Received: 29 August 2020 / *Accepted:* 22 October 2020 / *Published:* 31 October 2020

A numerical investigation was conducted on the steady-state electrochemical performance of an anode-supported solid oxide fuel cell (SOFC) with various design parameters and operating conditions. A zero-dimensional mathematical model illustrating the electrochemical characteristics of SOFCs was used in this paper. The simulated results showed good agreement with the experimental data. By using this model as a simulation, the steady-state electrochemical performances of SOFCs were studied. Additionally, how the electrode and electrolyte thicknesses, triple-phase boundary (TPB) length, operating temperature, and pressure affected the SOFC performance was investigated. In addition, the effect of the structural and operating parameters on overpotentials was studied. Combining the analyses on the structural and operating parameters, recommendations were provided for optimizing SOFC designs. This work provides systematic suggestions for improving the building of an SOFC electrochemical reaction mechanism model.

Keywords: solid oxide fuel cells, electrochemical reaction mechanism, three-phase boundary, polarization, parametric analysis

1. INTRODUCTION

In recent years, solid oxide fuel cells have been identified and increasingly studied as promising technology for clean and efficient power generation while alleviating environmental pollution[1-3]. As a solid-state energy conversion device, solid oxide fuel cells (SOFCs) can efficiently operate using a variety of fuels[4-5]. There are two kinds of SOFCs: planar and tubular[6]. Due to their long current paths, the power density of tubular SOFCs tends to be low. In contrast, the high power density output of planar SOFCs is high. Planar SOFCs can be divided into three categories: anode-supported, cathode-supported and electrolyte-supported[7]. In an electrolyte-supported SOFC, the ohmic resistance is very high because the electrolyte is thicker than the electrodes. Unfortunately, a cathode-supported design causes a high activation overpotential. Therefore, anode-supported designs have been widely used.

Mathematical models of heat/mass transfer in SOFCs have been developed[8-9]. These models all depend on the accurate prediction of the electrochemical parameters (such as the current density, output voltage, and power density) of the cell. Some researchers have studied the correlation between the thickness of the electrolyte or electrode and the overpotential of SOFCs[10]. In these studies, it is confirmed that the porosity and pore size of the electrode have little impact on the electrode exchange current density [11-13]. Therefore, the SOFC overpotentials are ambiguous in the existing models. In other models, the concentration overpotential is ignored because the rate of gas diffusion is assumed to be low when the temperature is low[14-16]. This hypothesis neglects the deep understanding of the concentration overpotential. In other studies, the model works after considering the activation, concentration, and ohmic overpotential as a total resistance because the three overpotentials vary with the operating parameters but without significant differences[17-19].

The physical and chemical processes that occur inside SOFCs are very complex. Large quantities of time and money can be consumed by conducting experiments to study SOFCs[20-22]. Thus, mathematical modeling is an essential tool in the exploration of SOFCs. A verified model not only provides a better illustration of an SOFC but can also be used to predict the effects of changing parameters; thus, the data can be used to optimize SOFC performance. Additionally, such a model can be used to examine the relative system sensitivity to relevant design parameters. In this paper, more precise and detailed modeling of the electrochemical performance of SOFCs is presented.

2. MATHEMATICAL MODEL FOR THE SOFC ELECTROCHEMICAL PERFORMANCE

The fundamental mechanisms of SOFC should be elucidated before simulating the performance of an SOFC. SOFCs operate at high temperatures and at atmospheric or elevated pressures. SOFCs can use not only hydrogen but also carbon monoxide and hydrocarbons as fuel.

As illustrated in Fig. 1, oxygen (air) and fuel gas (hydrogen) are fed to the cathode and anode, respectively. At the anode side, hydrogen molecules diffuse to the triple-phase boundary (TPB). The oxygen molecules diffuse through the porous cathode to the TPB, where they form oxygen ions after receiving electrons. Additionally, the flow of electrons transported to the cathode produces direct-current electricity via an external circuit.

There are many complex physical and chemical transformations in SOFCs. To make the calculation more feasible, it should be noted that some assumptions are made in the process of modeling: the pressure drop between the inlet and outlet of the flow channel is negligible, the temperature is uniform and the model is isothermal, and the gases both at the anode and cathode sides have been considered to be ideal gases.

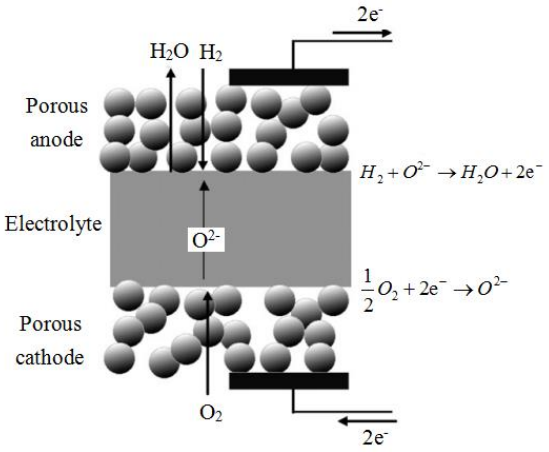

Figure 1. Schematic showing the SOFC mechanism

Due to the effect of different overpotentials, the operating voltage of SOFCs is much lower than the open-circuit voltage. The total operating voltage of an SOFC can be expressed by the following equation[23]:

$$V = V_{nernst} - \left(\eta_{act,a} + \eta_{act,c} + \eta_{conc,a} + \eta_{conc,c} + \eta_{ohm}\right) \quad (1)$$

where V_{nernst} and η_{ohm} represent the Nernst voltage and ohmic overpotential, respectively, $\eta_{act,a}$ and $\eta_{act,c}$ are the activation overpotentials of the anode and cathode, respectively, and $\eta_{conc,a}$ and $\eta_{conc,c}$ represent the concentration overpotentials of the anode and cathode, respectively. The model for the SOFC electrochemical performance is shown in Fig. 2.

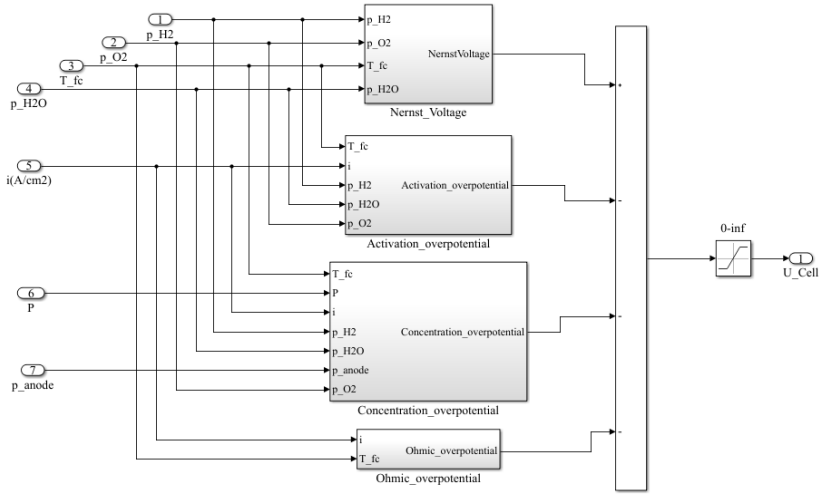

Figure 2. Model for the SOFC electrochemical performance

2.1 Nernst voltage

The Nernst equation is often used to express the electromotive force in SOFCs, which is caused by the difference between the thermodynamic potentials of electrode reactions[24-25].

$$V_{nernst} = E^0 + \frac{RT}{2F}\ln\left(\frac{P_{H_2}P_{O_2}^{0.5}}{P_{H_2O}}\right) \quad (2)$$

where R is the universal gas constant ($8.3145\,J\cdot mol^{-1}\cdot K^{-1}$); F is the Faraday constant ($9.6485\times10^{4}C\cdot mol^{-1}$); T is the absolute temperature; P_{H_2O}, P_{H_2} and P_{O_2} are the partial pressures of steam, hydrogen, and oxygen, respectively; and E^0 is the reversible potential, which is a function of the change in Gibbs free energy for hydrogen oxidation. The reversible potential at standard temperature and pressure can be obtained by the following equation:

$$E^0 = 1.253 - 2.4516\times10^{-4}T \tag{3}$$

2.2 Activation overpotential

Associated with electrode kinetics, the activation overpotential is generated in the electrochemical reaction region. The nonlinear Butler-Volmer equation is often used to describe the correlation between the current density and activation overpotential. The electrochemical reaction can be expressed by:

$$j = j_0\left[\exp\left(\alpha\frac{nF\eta_{act}}{RT}\right) - \exp\left(-(1-\alpha)\frac{nF\eta_{act}}{RT}\right)\right] \tag{4}$$

where j_0 stands for the electrode exchange current density; α is the symmetrical factor, which is always set to 0.5 for SOFCs; and n stands for the electron number of every reaction, which is always set to 2 for SOFCs[26]. The activation overpotential can be written as:

$$\eta_{act,i} = \frac{RT}{F}\sinh^{-1}\left(\frac{j}{2j_{0,\mathrm{i}}}\right) = \frac{RT}{F}\ln\left[\frac{j}{2j_{0,\mathrm{i}}} + \sqrt{\left(\frac{j}{2j_{0,i}}\right)^2 + 1}\right], i = a, c \tag{5}$$

where $\eta_{act,a}$ and $\eta_{act,c}$ represent the anode and cathode activation overpotentials, respectively, $J_{0,i}$ is the exchange current density that represents the readiness of an electrode to proceed with an electrochemical reaction, and the subscripts *a* and *c* represent the anode and cathode, respectively[27]. The value of $J_{0,i}$ is closely associated with the sensitively of the activation overpotential to the operating conditions. Usually, the exchange current density can be written as:

$$j_{0,a} = \gamma_a L_{\mathrm{tpb}}\left(\frac{P_{H_2}}{P_{ref}}\right)\left(\frac{P_{H_2O}}{P_{ref}}\right)\exp\left(-\frac{E_{act,a}}{RT}\right) \tag{6}$$

$$j_{0,C} = \gamma_C L_{\mathrm{tpb}}\left(\frac{P_{O_2}}{P_{ref}}\right)^{0.25}\exp\left(-\frac{E_{act,C}}{RT}\right) \tag{7}$$

where L_{tpb} stands for the length of the TPB, $E_{act,c}$ and $E_{act,a}$ stand for the cathode and anode activation energies, respectively, γ_c and γ_a represent the cathode and anode exchange current density coefficients, respectively, and P_{ref} is the reference pressure (1 bar).

2.3 Concentration overpotential

Due to the resistance caused by species diffusion through the electrolyte to the reaction site, a concentration overpotential occurs. The molecular transport of gas species in electrode pores, along with reactants dissolving in the electrolyte and the products precipitating out of the electrolyte, all affect the concentration overpotential. An SOFC has a three-layer positive-electrolyte-negative (PEN) structure. A PEN structure is composed of an anode electrode, an electrolyte and a cathode electrode. For an anode-

supported SOFC with a PEN structure, the concentration overpotential is usually significant at the anode. Furthermore, it becomes more obvious when SOFCs are operated in the high current density region[28]. The concentration overpotential of the anode and cathode can be expressed by:

$$\eta_{conc,c} = \frac{RT}{2F}\ln\left(\frac{P^l_{H_2}\cdot P_{H_2O}}{P_{H_2}\cdot P^l_{H_2O}}\right) \tag{8}$$

$$\eta_{conc,a} = \frac{RT}{2F}\ln\left(\frac{P^l_{O_2}}{P_{O_2}}\right)^{\frac{1}{2}} \tag{9}$$

where P^l stands for the partial pressures at the TPB. Since the gas transport in the pore selection layer is mainly in the form of diffusion, the Fick model can be used to determine the partial pressure at the electrode-electrolyte interface. Therefore, the relationship between the partial pressures of H_2, H_2O, and O_2 at the three-phase boundaries can be expressed as:

$$P^l_{H_2} = P_{H_2} - \frac{jRT\delta_{anode}}{2FD_{eff,anode}} \tag{10}$$

$$P^l_{H_2O} = P_{H_2O} + \frac{jRT\delta_{anode}}{2FD_{eff,anode}} \tag{11}$$

$$P^l_{O_2} = P - \left(P - P_{O_2}\right)\exp\left(\frac{jRT\delta_{cathode}}{4FPD_{eff,cathode}}\right) \tag{12}$$

where $\delta_{cathode}$ and δ_{anode} are the thicknesses of the cathode and anode, respectively and $D_{eff,cathode}$ and $D_{eff,anode}$ represent the effective diffusivity coefficients of the cathode and anode, respectively. The effective diffusion coefficients of the anode and cathode in an SOFC can be written as:

$$D_{eff,anode} = \left(\frac{P_{H_2O}}{P_{an}}\right)D_{H_2,eff} + \left(\frac{P_{H_2}}{P_{an}}\right)D_{H_20,eff} \tag{13}$$

$$D_{eff,cathode} = D_{O_2,eff} \tag{14}$$

where $D_{H_2,eff}$, $D_{H_2O,eff}$ and $D_{O_2,eff}$ are the effective diffusivities of H_2, H_2O, and O_2, respectively. The diffusion in porous electrodes is mainly based on two mechanisms, namely, molecular diffusion and Knudsen diffusion. Molecular diffusion dominates when the pore size is much larger than the mean free path of steam molecules. In contrast, the interaction between molecules and pore walls is the dominant mechanism that contributes to Knudsen diffusion. Due to the existence of both mechanisms, the effective diffusion coefficient of H_2, H_2O and O_2 can be written using the Bosanquet formula[29-30],

$$D_{H_2,eff} = \frac{\varepsilon}{\tau}\left(\frac{1}{D_{H_2-H_2O}} + \frac{1}{D_{H_2,k}}\right)^{-1} \tag{15}$$

$$D_{H_2O,eff} = \frac{\varepsilon}{\tau}\left(\frac{1}{D_{H_2-H_2O}} + \frac{1}{D_{H_2O,k}}\right)^{-1} \tag{16}$$

$$D_{O_2,eff} = \frac{\varepsilon}{\tau}\left(\frac{1}{D_{O_2-N_2}} + \frac{1}{D_{O_2,k}}\right)^{-1} \tag{17}$$

where ε stands for the tortuosity of the anode material, τ is the porosity of the anode material, $D_{H_2-H_2O}$ stands for the effective molecular diffusion coefficient of a H_2-H_2O binary system, $D_{O_2-N_2}$ stands for the effective molecular diffusion coefficient of a O_2-N_2 binary system, and $D_{H_2,k}$, $D_{H_2O,k}$ and $D_{O_2,k}$ are the effective Knudsen diffusion coefficients for H_2, H_2O and O_2, respectively. The effective molecular diffusion coefficient can be estimated using the Fuller equation[31-32]:

$$D_{i-j} = \frac{0.00143T^{1.75}}{pM_{ij}^{0.5}\left[\left(\sum v\right)_i^{1/3} + \left(\sum v\right)_j^{1/3}\right]^2} \quad (18)$$

$$D_{i,k} = 48.5 d_p \left(\frac{T}{M_i}\right)^{0.5} \quad (19)$$

where $M_{ij} = 2\left[\left(1/M_i\right) + \left(1+M_j\right)\right]^{-1}$, M stands for the molecular weight[33]; $\sum_v$ stands for the diffusion volume of different species (6.12 for H_2, 13.1 for H_2O, 16.3 for O_2 and 18.5 for N_2), $D_{i,k}$ is the Knudsen diffusion coefficient; and d_p stands for the mean pore diameter (1×10^{-6} m).

2.4 Ohmic overpotential

The ohmic overpotential, which is of great importance for SOFCs, is proportional to the current density. It is caused by the conduction resistance of ions and electrons and the contact resistance between cell components. Therefore, the ohmic overpotential can be calculated based on the ohm law:

$$\eta_{ohm} = jR_{ohm} \quad (20)$$

where R_{ohm} stands for the internal resistance of the SOFC, which consists of the electron and ion resistances; and j stands for the current density. R_{ohm} can be determined using the effective distance between cell components coupled with conductivity data. It is assumed that the contact and interaction resistance can be negligible. Therefore, R_{ohm} can be calculated using the following equation:

$$R_{ohm} = \frac{\delta_{anode}}{\sigma_{anode}} + \frac{\delta_{electrolyte}}{\sigma_{electrolyte}} + \frac{\delta_{cathode}}{\sigma_{\mathrm{cathode}}} \quad (21)$$

$$\sigma_{anode} = \frac{9.5\times10^7}{T}\exp\left(\frac{-1150}{T}\right) \quad (22)$$

$$\sigma_{cathode} = \frac{4.2\times10^7}{T}\exp\left(\frac{-1200}{T}\right) \quad (23)$$

$$\sigma_{electrolyte} = 3.34\times10^4 \exp\left(\frac{-10300}{T}\right) \quad (24)$$

where $\sigma_{cathode}$ and σ_{anode} are the electronic conductivities of the cathode and anode ($\Omega^{-1}m^{-1}$), respectively, $\sigma_{electrolyte}$ is the ionic conductivity of the electrolyte ($\Omega^{-1}m^{-1}$), and δ stands for the thicknesses of the electrodes and electrolyte.

2.5 Model validation

To verify the accuracy and feasibility of the model, some of the simulation results are compared with the experimental results of the model. Table 1 shows the physical parameters and operating conditions of the experiment and simulation.

Table 1. Physical parameters and operating conditions[34-37]

Physical parameters and operating conditions	Values
Pre-exponential factor of the anode exchange current density, γ_a (A/m^2)	1.344×10^{10}

Pre-exponential factor of the cathode exchange current density, γ_c (A/m^2)	2.051×10^9
Activation energy of the anode, $E_{act,a}$ (J/mol)	1.0×10^5
Activation energy of the cathode, $E_{act,c}$ (J/mol)	1.2×10^5
Anode porosity, ε	0.45
Anode tortuosity, τ	3.5
Length of the TPB, L_{tpb} (μm)	1
Anode thickness, δ_{anode} (μm)	400
Cathode thickness, $\delta_{cathode}$ (μm)	30
Electrolyte thickness, $\delta_{electrolyte}$ (μm)	20
Operating temperature, T (K)	1023
Operating pressure, P (bar)	1.2

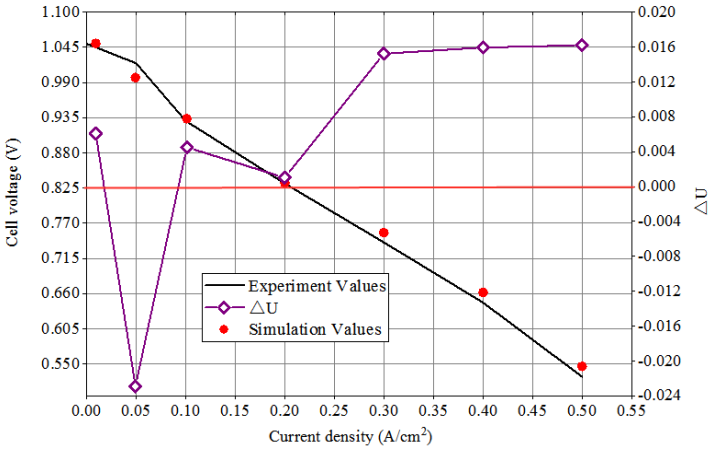

Figure 3. Comparison between the experimental data and simulated values

As shown in Fig. 3, the simulation values based on the model are compared with the experimental data[38], and ΔU is the value of the simulation value minus the experimental value. The I-V curve shows that the simulated values agree well with the experimental data. In fact, when an SOFC is at the start-up stage, the physical and chemical reactions are not stable. It can be seen from the figure that the errors are more significant when the current density is lower than 0.3 A/cm^2. At this time, the voltage value can easily be affected by many factors (such as ohmic heating and the sudden variations in molar concentrations), which may explain this discrepancy. Nonetheless, the maximal error is no more than 5%, which indicates the sufficient accuracy of the model to investigate the SOFC electrochemical performance.

3. RESULTS AND DISCUSSION

The overpotentials of SOFCs are strongly related to the structural and operating parameters, which is of great significance for optimizing SOFC designs. Therefore, the validated model above was used to simulate the steady-state electrochemical performance of SOFCs with different structural

parameters (Section 3.1) and operating conditions (Section 3.2), and the effect of every factor could be entirely analyzed.

3.1 Effect of the structural parameters of the cell

In this section, the effect of different design parameters (the electrolyte, anode, and cathode thicknesses, and the length of TPB) on the steady-state electrochemical performance of SOFCs is introduced by simulating the model.

3.1.1 Electrolyte thickness effect

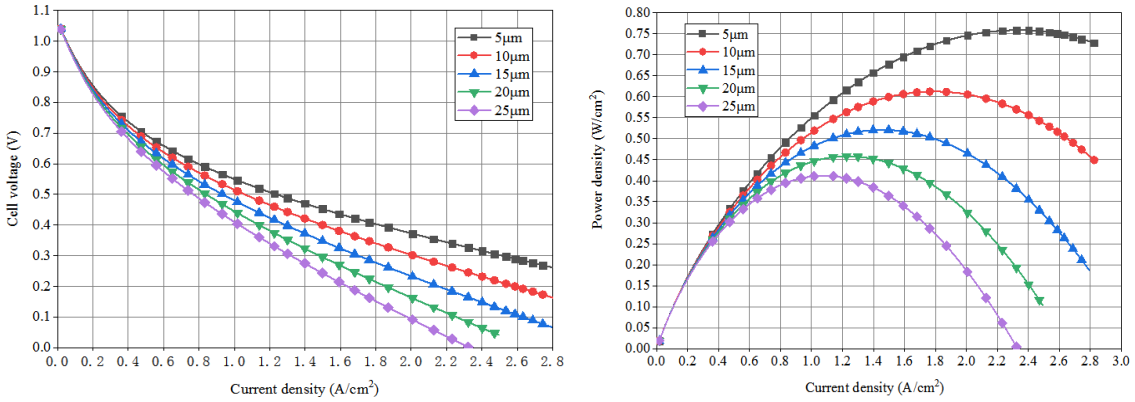

(a) (b)

Figure 4. Effect of the electrolyte thickness on (a) the cell voltage and (b) power density

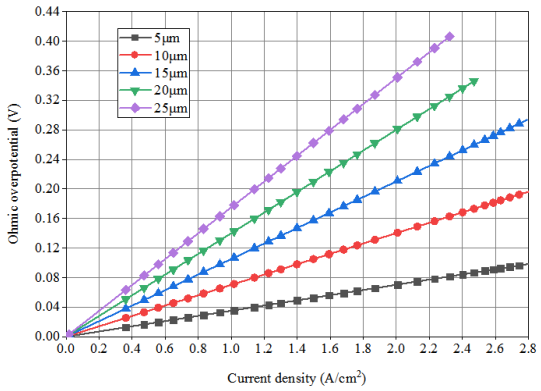

Figure 5. Effect of the electrolyte thickness on the ohmic overpotential

Fig. 4(a) demonstrates that the cell voltage decreases severely as the electrolyte thickness increases. The change is particularly evident in the high potential region. Fig. 4(b) shows that the power density improves significantly as the electrolyte thickness decreases. At the same time, the maximum power density shifts to higher values as the electrolyte thickness decreases. Li *et al.*[39] found the variation in the voltage and power of tubular SOFCs was close to the tendency studied in this work. The effect of the electrolyte thickness applies to both types of SOFCs. However, this result is nonsignificant

in the high potential region. Therefore, with the decrease in electrolyte thickness, the SOFC can work at a high current density. This result occurs because the resistance of the electrolyte is proportional to its thickness; thus, the thickness of the electrolyte plays a significant role in the output power of an SOFC.

According to Fig. 5, the ohmic overpotential increases with increasing electrolyte thickness, which is consistent with the above analysis. With the increase in electrolyte thickness, the diffusion distance for oxygen ions moving through oxygen vacancies increases. Therefore, the resistance of oxygen ion transmission increases. The high internal resistance loss of SOFCs will inevitably lead to a decrease in their output power. Consequently, a decrease in electrolyte thickness is helpful for improving the electrochemical performance of SOFCs.

3.1.2 Anode thickness effect

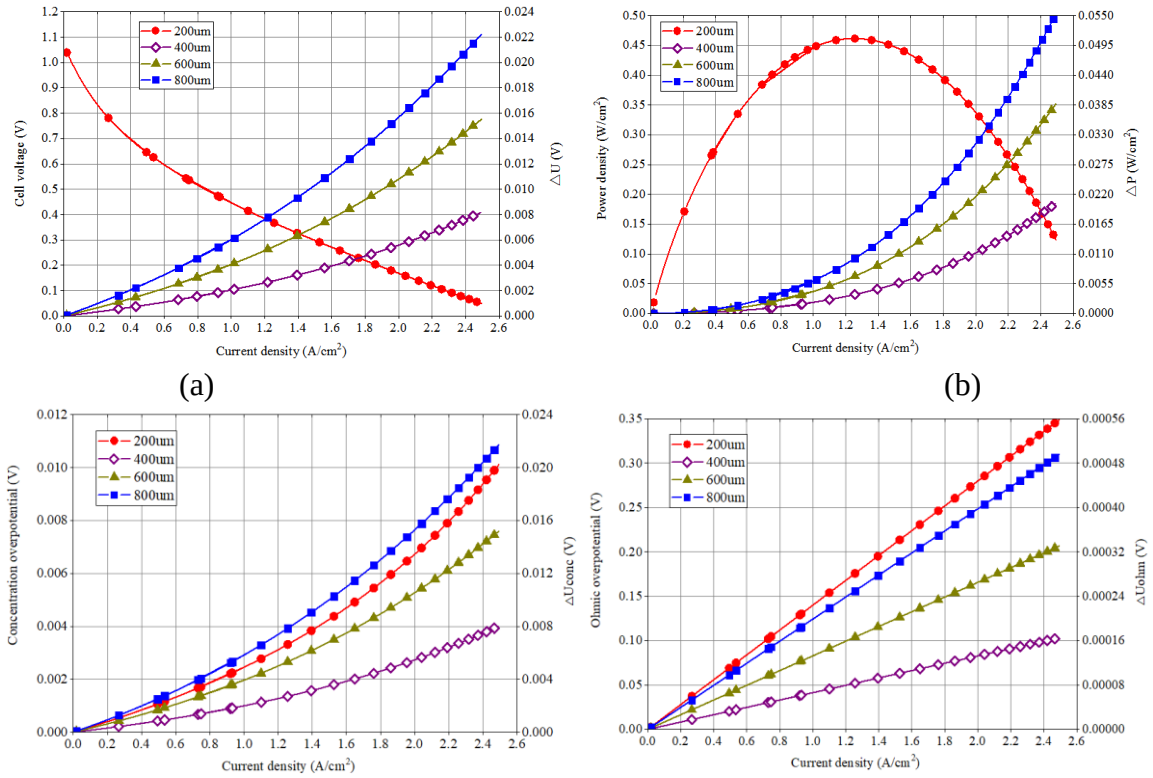

Figure 6. Effect of the anode thickness on (a) the cell voltage, (b) power density, (c) concentration overpotential, and (d) ohmic overpotential

$$\Delta U = U_{200\mu m} - U_i, i = 400\,\mu m, 600\,\mu m, 800\,\mu m \quad (25)$$

$$\Delta P = P_{200\mu m} - P_i, i = 400\,\mu m, 600\,\mu m, 800\,\mu m \quad (26)$$

$$\Delta U_{conc} = U_{conc,i} - U_{conc,20\mu m}, i = 400\,\mu m, 600\,\mu m, 800\,\mu m \quad (27)$$

$$\Delta U_{ohm} = U_{ohm,i} - U_{ohm,200\mu m}, i = 400\,\mu m, 600\,\mu m, 800\,\mu m \quad (28)$$

where $U_{200\mu m}$, $P_{200\mu m}$ and $U_{ohm,200\mu m}$ represent the cell voltage, power density, and ohmic overpotential, respectively, of an SOFC with an anode thickness of a 200 μm. Although Fig. 6(a) and (b) show that the effect of anode thickness on the cell voltage and power density is insignificant, respectively, the

electrochemical performance increases with a decrease in anode thickness. By comparing Fig. 6(a) and (b) with Fig. 4(a) and (b), respectively, the influence of the anode thickness on the cell voltage and power density is less than the observed influence of the electrolyte thickness. Fig. 6(c) and (d) show that an increasing anode thickness causes an increase in both the concentration and ohmic overpotentials, which is more evident at a high current density. The ohmic concentration increases slightly with an increasing anode thickness. However, the concentration overpotential increases significantly. The research of Marco *et al.*[40] showed that SOFCs with a large anode/electrolyte thickness ratio had a positive influence on electrolyte densification when the operating temperature (1173 K) was high. This result occurs because the diffusion of H_2 is inhibited at the TPB as the anode thickness increases. Moreover, the partial pressure of H_2O increases at the TPB. These circumstances account for the dramatic increase in the concentration overpotential.

3.1.3 Cathode thickness effect

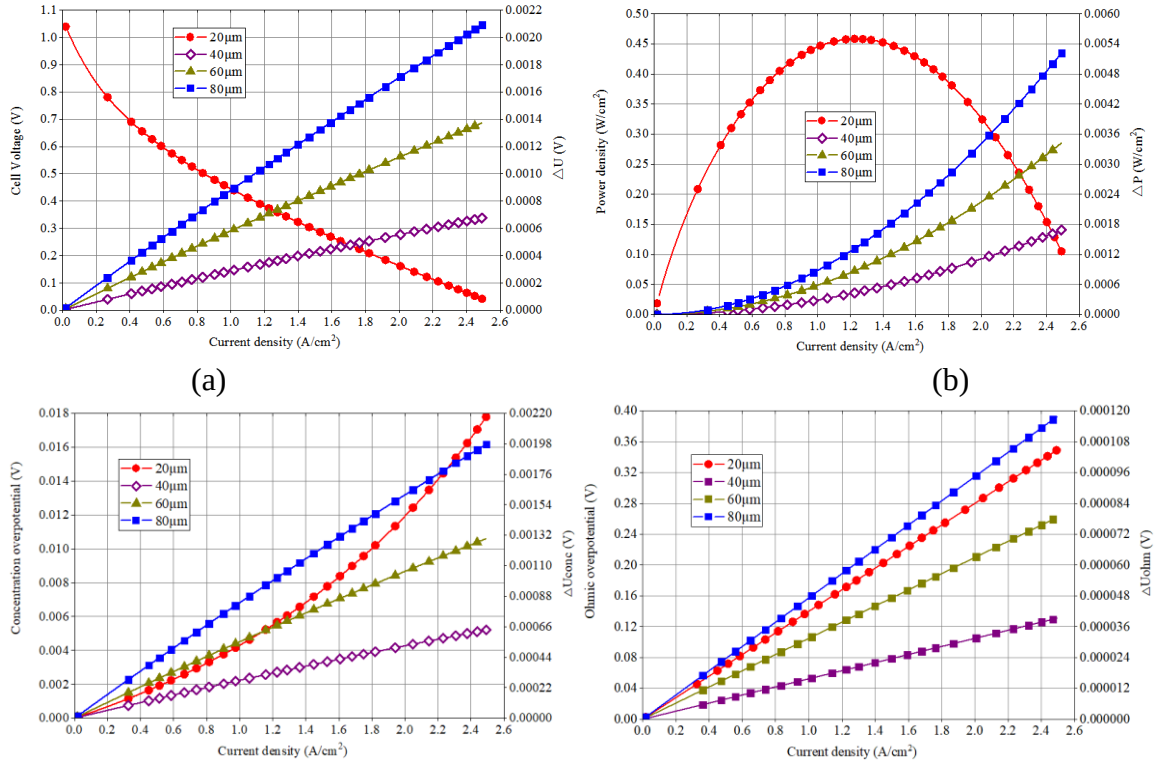

Figure 7. Effect of the cathode thickness on (a) the cell voltage, (b) power density, (c) concentration overpotential, and (d) ohmic overpotential

$$\Delta U = U_{20\mu m} - U_i, i = 40\mu m, 60\mu m, 80\mu m \quad (29)$$

$$\Delta P = P_{20\mu m} - P_i, i = 40\mu m, 60\mu m, 80\mu m \quad (30)$$

$$\Delta U_{conc} = U_{conc,i} - U_{conc,20\mu m}, i = 40\mu m, 60\mu m, 80\mu m \quad (31)$$

$$\Delta U_{ohm} = U_{ohm,i} - U_{ohm,20\mu m}, i = 40\mu m, 60\mu m, 80\mu m \quad (32)$$

where $U_{20\mu m}$, $P_{20\mu m}$, $U_{conc,20\mu m}$ and $U_{ohm,20\mu m}$ represent the cell voltage, power density, concentration overpotential, and ohmic overpotential, respectively, of an SOFC with a cathode thickness of 20 μm.

Comparing Fig. 7(a) and (b) with Fig. 4(a) and (b), respectively, it is evident that the effect of the cathode thickness on the cell voltage and power density is less than the effect of the electrolyte thickness. As the cathode thickness increases, the ohmic and concentration overpotentials increase. The reason for this is that the diffusion of O_2 is inhibited at the TPB as the anode thickness increases. Additionally, the partial pressure of H_2O increases at the TPB. These circumstances account for the dramatic increase in the concentration overpotential.

3.1.4 TPB length effect

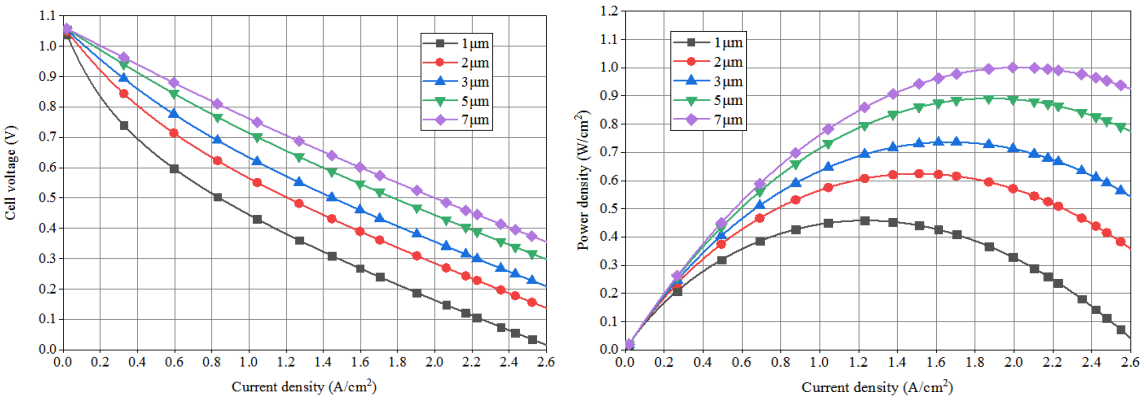

(a) (b)

Figure 8. Effect of the TPB length on (a) the cell voltage and (b) power density

As a significant microstructural component of SOFCs, the TPB length greatly influences cell performance[41]. Fig. 8(a) and (b) show that the cell voltage and power density both increase with an increasing TPB length. The value of the maximum power density is higher with a long TPB length. Therefore, the electrochemical performance of SOFCs is improved with an increasing TPB length, which stems from the simultaneous increase in the electrode current density.

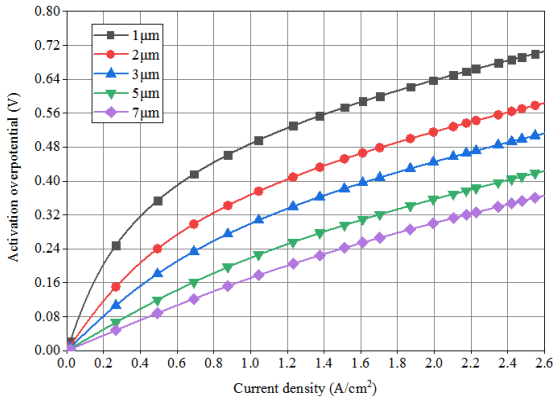

Figure 9. Effect of the TPB length on the activation overpotential

Fig. 9 demonstrates that the decrease in the TPB length causes a significant increase in the activation overpotential. The value of the activation overpotential increases dramatically at a low current density, which causes a significant drop in cell voltage (see Fig. 8(a)). As the length of the TPB decreases, this phenomenon becomes increasingly obvious. The activation overpotential mainly depends on the electrode porosity, particle diameter, and volume fraction of the electronic and ionic phases. These factors determine the length of the TPB. Thus, the activation overpotential is closely related to the length of the TPB.

3.2 Effect of the operating conditions

In this section, the effect of different operating temperatures or pressures on the SOFC overpotential is studied. Additionally, the simulated curves of the output voltage and power density in regard to the current density are analyzed.

3.2.1 Operating temperature effect

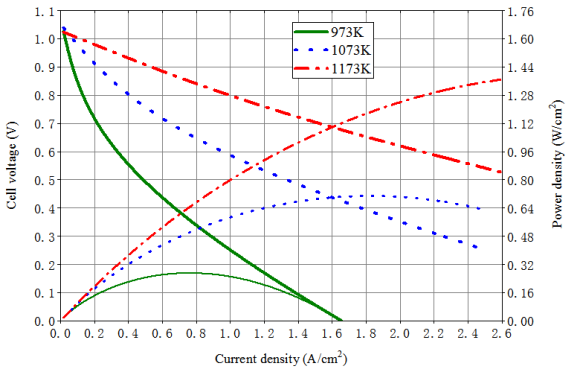

Figure 10. Effect of the operating temperature on the cell voltage and power density

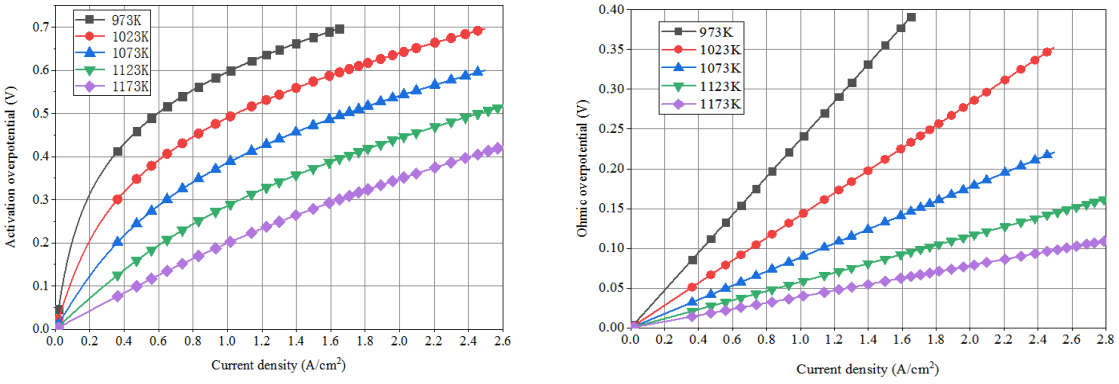

(a) (b)

Figure 11. Effect of the operating temperature on (a) the activation overpotential and (b) ohmic overpotential

As shown in Fig. 10, the cell voltage and power density gradually increase with an increasing operating temperature. This result is particularly apparent at a high current density. Based on a neural network model to predict the electrochemical characteristics of SOFCs, Chaichana *et al.*[42] obtained

the variation in the voltage and power density when the operating temperature was as low as 800 K. At low temperatures, the mobility of oxygen ions in the electrolyte is low, causing the low conductivity of the electrolyte. Therefore, the internal resistance of the fuel cell is considerably higher. Most of the power consumption of SOFCs is consumed by the internal resistance. With an increasing temperature, the electrolyte resistance decreases, and the catalytic activity of the electrode increases. These factors promote the electrochemical reaction of SOFCs. Fig. 11(a) and (b) display that both the activation and ohmic overpotentials decrease as the operating temperature increases. The conductivity of the material increases as the temperature increases, which is in accord with the description in the previous paragraph. Hence, the ohmic overpotential will gradually decrease.

3.2.2 Operating pressure effect

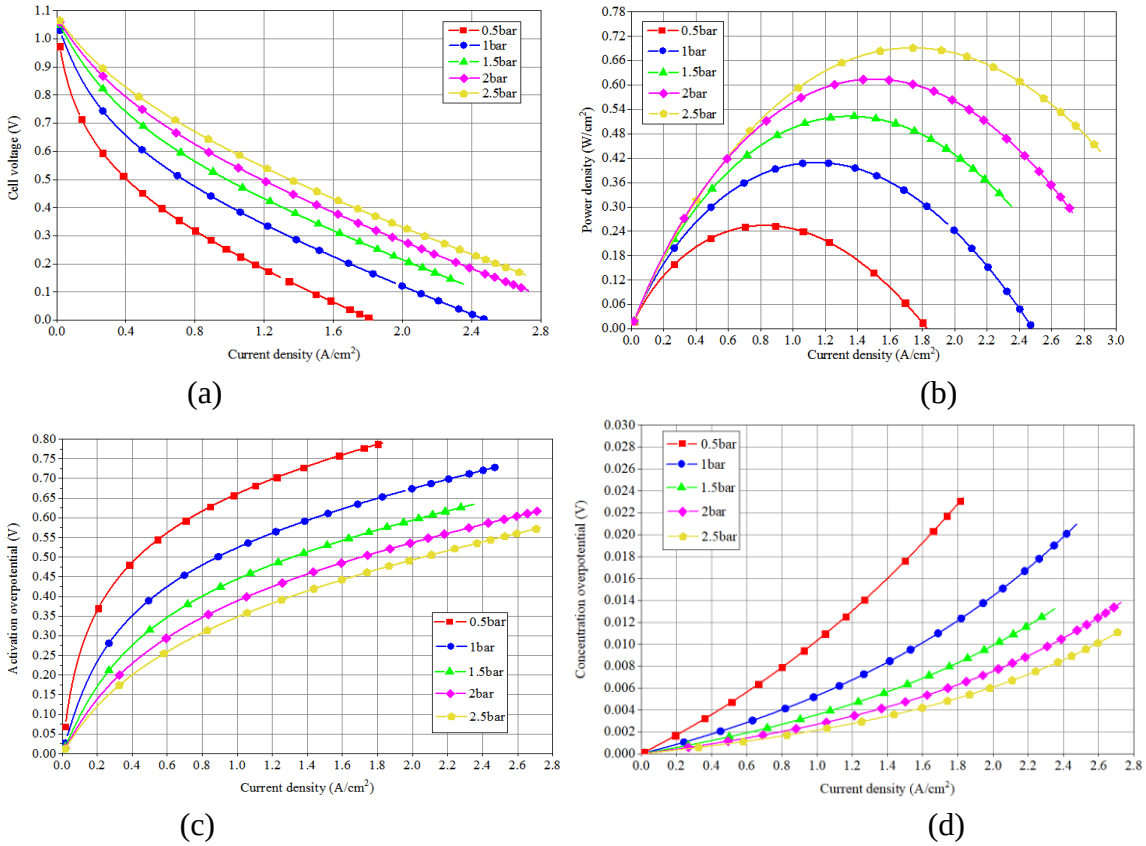

Figure 12. Effect of the operating pressure on (a) the cell voltage, (b) power density, (c) activation overpotential, and (d) concentration overpotential

It is evident from Fig. 12(a) and (b) that an increase in the operating pressure leads to an improvement in the electrochemical performance. Fig. 12(c) and (d) reveal that the activation and concentration overpotential decrease due to the increase in operating pressure. As shown in Fig. 12(a) and (b), the effect of operating pressure is less sensitive at high pressures (such as 1.5-2.5 bar). Pirkandi *et al.*[43] found a similar variation when the operating pressure of an SOFC was as low as 0.1 bar. This result occurs because the molar concentration at the electrode decreases as the operating pressure

decreases, which causes an increase in the activation overpotential. However, gas diffusion improves, which leads to a decreased concentration overpotential.

4. CONCLUSIONS

A mathematical model for anode-supported SOFCs was developed to investigate the steady-state electrochemical performance. The developed model consisted of the Nernst voltage and the activation, concentration, and ohmic overpotentials. Furthermore, these submodules were related to the operating and structural parameters. By using this model, the SOFC performance was analyzed.

Ohmic polarization is the cause of the most significant potential loss and is inversely proportional to the operating temperature. The operating temperature has a significant influence on the output voltage and power of an SOFC. Generally, increasing the temperature can increase the effective potential and output power of the fuel cell. However, due to the different thermal expansion rates of the electrode and electrolyte materials, the temperature should not be too high. Furthermore, a high operating temperature makes the thermal stability of the internal structure of the cell and the thermal management of SOFCs more difficult.

The ohmic overpotential is caused by the resistances of the electrodes and electrolyte. The effect of the resistances of the electrodes is negligible compared with the resistance of the electrolyte. Thus, the resistance of the electrolyte is the main part of the internal resistance of an SOFC. The influence of the electrolyte thickness on the electrochemical performance of SOFCs is much greater than that of the anode and cathode thicknesses. Decreasing the thickness of the electrolyte decreases the internal resistance loss of the electrolyte, which is an effective way to improve the current and power densities of SOFCs. Consequently, it is an effective way of improving the performance of SOFCs for studying the thin-film manufacturing technology of electrolytes or to develop new electrolyte materials with high conductivities. Additionally, it is of great help to improve the electrochemical performance of SOFCs by using suitable electrolyte and electrode materials and optimizing the operating conditions for the catalyst to improve the length of the TPB in SOFCs.

Increasing the operating pressure can increase the partial pressure of every reactant species, which leads to a decrease in the activation and concentration polarization and an increase in the reversible potential of an SOFC. However, increasing the operating pressure also increases the requirements of the material, structure, and sealing of SOFCs. Furthermore, an increase in the operating pressure will inevitably increase the power consumption of the air compressor.

ACKNOWLEDGMENTS
This work was supported by the Major Science and Technology Innovation Project in Shandong Province (2018CXGC0803).

References

1. S. Su, C. Yan, A. Kukolin and D. Chen, *Int. J. Electrochem. Sci.*, 14 (2019) 5226.
2. S. Elena and N. Truls, *Chem. Commun.*, 52 (2016) 1759.
3. J. Cao, Y. Liu, X. Huang and Y. Ji, *ACS Appl. Mater. Interfaces*, 10 (2018) 10528.
4. X. V. Nguyen, G. B. Jung and S. H. Chan, *Int. J. Electrochem. Sci.*, 14 (2019) 9132.
5. K. T. Lee, C. M. Gore and E. D. Wachsman, *J. Mater. Chem.*, 22 (2012) 22405.
6. R. J. Gorte, S. Park, J. M. Vohs and C. Wang, *Adv. Mater.*, 12 (2001) 1465.
7. K. Masahiro, T. Keita, Y. Shun, Y. Yuki, T. Takayuki and S. Kazuya, *ECS Trans.*, 68 (2015) 2831.
8. L. Barelli, G. Bidini and A. Ottaviano, *Applied Energy*, 110 (2013) 173.
9. C. Bao, Y. Wang, D. Feng, Z. Jiang and X. Zhang, *Prog. Energy Combust. Sci.*, 66 (2018) 83.
10. H. A. Ozgoli, M. Moghadasi, F. Farhani and M. Sadigh, *Environ. Prog. Sustainable Energy*, 36 (2017) 610.
11. K. Mihails, T. Nikolai, M. Martin and M. Alexander, *Materials*, 9 (2016) 906.
12. K. Q. Zheng, M. Ni, Q. Sun and L. Y. Shen, *Acta Mech. Sin.*, 29 (2013) 388.
13. N. Tímea, H. Douglas and B. Dezso, *J. Phys. Chem. B*, 115 (2011) 11409.
14. W. Tong, K. Somasundaram, E. Birgersson, A. S. Mujumdar and C. Yap, *Appl. Therm. Eng.*, 99 (2016) 672.
15. A. Nakajo, F. Mueller, J. Brouwer, J. V. herle, D. Favrat, *Int. J. Hydrogen Energy*, 37 (2012) 9249.
16. D. Klotz, A. Leonide, A. Weber and E. Ivers-Tiffée, *Int. J. Hydrogen Energy*, 39 (2014) 20844.
17. Meng Ni, M. K.H. Leung and D. Y. C. Leung, *Chem. Eng. Technol.*, 31 (2008) 1319.
18. S. A. Hajimolana, M. A. Hussain, M. Soroush, W. M. A. Wan Daud and M. H. Chakrabarti, *Fuel Cells*, 12 (2012) 761.
19. W. H. Kan and V. Thangadurai, *Ionics*, 21 (2015) 301.
20. V. Cascos, R. Martínez-Coronado, J. A. Alonso and M. T. Fernández-Díaz, *ACS Appl. Mater. Interfaces*, 6 (2014) 9194.
21. K. J. Pan, A. M. Hussain and E. D. Wachsman, *J. Power Sources*, 347 (2017) 277.
22. E. M. Kck, M. Kogler, B. Kltzer, M. F. Noisternig, S. Penner, *ACS Appl. Mater. Interface*s, 8 (2016) 16428.
23. T. Yang, H. Sezer, I. Celik, H. Finklea and K. Gerdes, *Int. J. Electrochem. Sci.*, 12 (2017) 6801.
24. G. A. Hughes, J. G. Railsback, K. J. Yakal-Kremski, D. M. Butts and S. A. Barnett, Faraday Discuss., 182 (2015).
25. P. Aguiar, C.S. Adjiman and N.P. Brandon, *J. Power Sources*, 138 (2004) 120.
26. M. Ni, M. K. H. Leung and D. Y. C. Leung, *Chem. Eng. Technol.*, 29 (2006) 636.
27. I. S. Averkov, A. V. Baykov, L. S. Yanovskiy and V. M. Volokhov, *Russ. Chem. Bull.*, 65 (2016) 2375.
28. M. Ni, M. K. H. Leung and D. Y. C. Leung, *Energy Convers. Manage.*, 48 (2007) 1525.
29. Z. Barbara, P. Oprych, Paulina, Jaworski and Zdzislaw, *Chem. Ing. Tech.*, 86 (2014).
30. A. A. AlZahrani and I. Dincer, *Int. J. Hydrogen Energy*, 42 (2017) 21404.
31. C. Bao, Z. Jiang and X. X. Zhang, *J. Power Sources*, 310 (2016) 32.
32. W. Kong, Q Zhang, X Gao, J.Y. Zhang, D. Chen and S. Su, *Int. J. Electrochem. Sci.*, 10 (2015) 5800.
33. S. Su, S. Zhang, C. Yan, Z. Yang, F. Zheng and L. Zhang, *Int. J. Electrochem.* Sci., 12 (2017) 230.
34. V. I. Nikitsin and B. Backiel-Brzozowska, *Int. J. Heat Mass Transfer*, 56 (2013) 30.
35. S. Su, X. Gao, Q. Zhang, W. Kong and D. Chen, *Int. J. Electrochem. Sci.*, 10 (2015) 2487
36. H. C. Zhang, J.C. Chen and J.J. Zhang, *Int. J. Hydrogen Energy*, 38 (2013) 16354.
37. S. D. Ebbesen and M. Mogensen, *J. Power Sources*, 193 (2009) 349.
38. H. R. Amedi, B. Bazooyar and M. R. Pishvaie, *Energy*, 90 (2015) 605.
39. C. J. Li, C. X. Li, Y. Z. Xing, M. Gao and G. J. Yang, *Solid State Ionics*, 177 (2006) 2065.
40. V. D. Marco, A. Iannaci, S. Rashid and V. M. Sglavo, *Int. J. Hydrogen Energy*, 42 (2017) 12543.
41. P. Vijay, M. O. Tadé, Z. Shao and M. Ni, *Int. J. Hydrogen Energy*, 42 (2017) 28836.

42. K. Chaichana, Y. Patcharavorachot, B. Chutichai, D. Saebea, S. Assabumrungrat and A. Arpornwichanop, *Int. J. Hydrogen Energy*, 37 (2011) 2498.
43. J. Pirkandi, M. Ghassemi, M. H. Hamedi and R. Mohammadi, J. *Cleaner Prod.*,29 (2012) 151.